Available online at www.sciencedirect.com
SCIENCE DIRECT®
Journal of Catalysis 232 (2005) 257–267
JOURNAL OF CATALYSIS
www.elsevier.com/locate/jcat

Direct synthesis of methyl isobutyl ketone in gas-phase reaction over palladium-loaded hydroxyapatite

Nabil Cheikhi [a], Mohamed Kacimi [a], Mohamed Rouimi [a], Mahfoud Ziyad [a,*], Leonarda F. Liotta [b], Giuseppe Pantaleo [c], Giulio Deganello [b,c]

[a] *Faculté des Sciences, Laboratoire de Physico-Chimie des Matériaux et Catalyse, Département de chimie, Rabat, Morocco*
[b] *ISMN-CNR, via Ugo La Malfa 153, 90146 Palermo, Italy*
[c] *Dipartimento di Chimica Inorganica e Analitica, S. Cannizzaro, Università degli Studi, Viale delle Scienze, 90128 Palermo, Italy*

Received 13 January 2005; revised 16 March 2005; accepted 21 March 2005
Available online 22 April 2005

Abstract

Several compositions of palladium-loaded calcium hydroxyapatite Pd(x)/CaHAp were prepared and characterized by XRD, IR, and UV–visible spectroscopy and temperature-programmed reduction (TPR). The acid–base properties of the samples were studied with the use of butan-2-ol conversion and IR spectroscopy coupled with lutidine adsorption/desorption. Calcium hydroxyapatite bears Lewis acid sites of moderate strength and a limited number of Brønsted acid sites, which produce butenes by dehydration. The selectivity of the dehydrogenation reaction (formation of methyl ethyl ketone) is very limited in the absence of oxygen but indicates the existence on the surface of phosphate of basic sites that are as essential as the acid sites in the direct synthesis of methyl isobutyl ketone (MIBK) from acetone and H_2. Dispersion of Pd on the hydroxyapatite introduces redox properties and the bifunctionality needed in the hydrogenation of mesityl oxide (MO). Temperature-programmed reduction (TPR) of Pd(x)/CaHAp catalysts shows a sharp peak of H_2 consumption between 268 and 276 K, depending on palladium loading, followed by a negative peak at about 338 K, which is associated with the decomposition of β-PdH. Hydrogen chemisorption measurements carried out at 353 K allowed the determination of the size of palladium particles, which varies between 8 and 28 nm. The Pd(x)/CaHAp catalysts showed good performance in the low-pressure one-step synthesis of MIBK. They are stable under the experimental conditions, and they exhibit a MIBK and MIBC selectivity that reaches 92% for a conversion of 22% and an optimal Pd loading of 2 wt%. Other parameters of the reaction (such as temperature of reaction, residence time, H_2/acetone ratio) were studied. They all play an important role in acetone conversion and product distribution. However, the reaction temperature has the most significant influence, since a maximum of the global conversion was observed at 423 K.

Keywords: Calcium hydroxyapatite; Palladium catalysts; UV–visible-NIR diffuse reflectance; Butan-2-ol conversion; Temperature-programmed reduction; Methyl isobutyl ketone (MIBK) synthesis

1. Introduction

Methyl isobutyl ketone (MIBK or 4-methyl-2-pentanone) is an excellent solvent used in several industrial processes, such as paint production, cellulose treatment, initiation of polymerization, reagent in heavy metal extraction, and dewaxing of mineral oils [1]. MIBK synthesis is carried out via a three-step liquid-phase process [2]. In the first step acetone is condensed (aldolization) into diacetone alcohol (DAA) on a basic catalyst. In the second step the DAA is dehydrated with an acid into mesityl oxide (MO). The third step is limited to the dehydrogenation of MO over a metallic phase to produce MIBK. This three-step process has several disadvantages, which are shared by many other liquid-phase industrial syntheses. Liquid acids create corrosion problems and environmental pollution because their removal from the reaction mixture is expensive and is not easy to achieve. The

* Corresponding author. Fax: +212 37 77 56 34.
E-mail address: ziyad@fsr.ac.ma (M. Ziyad).

0021-9517/$ – see front matter
doi:10.1016/j.jcat.2005.03.016

process also produces undesirable products in the first two steps [3]. For all of these reasons, particular attention has been devoted in recent years to the search for a MIBK synthesis method that takes only one step and uses multifunctional solid catalysts. Moreover, the replacement of liquid acids and bases with their solid homologues has become an imperative to meet ecological requirements.

The literature has reported different studies of the MIBK synthesis with a steep process in liquid-phase and palladium- (or platinum-) loaded basic metallic oxides or oxides modified by a base such as KOH/Al_2O_3, MgO/SiO_2, and MgO/Nb_2O_5 [4,5]; cation exchange resins; and zirconium phosphate. Selectivities approaching 90% were obtained at high pressures. The literature has also reported several investigations carried out at atmospheric pressure, in gas phase, with catalysts containing Ni [6], Pt [7], or Pd [3,8–11] supported by HZSM5, MgO [8], and mixed oxides such as hydrotalcites [6,10,11]. In most cases the MIBK yield decreases rapidly during the first hours of reaction.

Despite their numerous features the phosphates were rarely used in this class of reaction [12]. Calcium hydroxyapatite (CaHAp), with its basic character, has been utilized in many domains but was never tested in MIBK synthesis [13–15]. It is also known as a cation exchanger and is active in dehydrogenation reactions. Copper-exchanged hydroxyapatite has been used industrially in chlorobenzene hydration [16] despite its rapid loss of activity due to the reduction of Cu^{2+} ions to metallic copper. Concomitantly, the OH^- ions are replaced in the phosphate framework by Cl^-, leading to a more stable solid. Hydroxyapatite was also used as Ni–Mo carrier in hydrodesulfuration reactions. Elazarifi et al. showed that the Mo–Co-loaded calcium hydroxyapatite has a catalytic activity comparable to that of conventional catalysts [17].

The hydroxyapatite $Ca_{10}(PO_4)_6(OH)_2$ is the main inorganic constituent of natural bone. Its structure was first resolved in 1930 by Naray-Szabo [18] and then refined by Beevers and McInter [19]. It crystallizes in the hexagonal system and belongs to the $P6_{3/m}$ (C_{6h}) space group. The framework of $Ca_{10}(PO_4)_6(OH)_2$ can be described as a compact assemblage of tetrahedral PO_4 groups that delimit two types of unconnected channels. The first one has a diameter of 2.5 Å and is bordered by Ca^{2+} ions (denoted Ca(I)). The second type plays an important role in the properties of the apatites. It has a diameter of around 3.5 Å and is also delimited by oxygen and Ca^{2+} ions in a coordination of 7 (denoted Ca(II)). These channels host $(OH)^-$ groups (or other halogens) along the c axis to balance the positive charge of the matrix. The apatite structure also possesses a great flexibility in accepting substitutions in its network and cationic exchanges (Ca^{2+}/M^{2+}) of calcium ions [20,21].

The present work is devoted to the investigation of the behavior of palladium-loaded hydroxyapatite in acetone condensation into MIBK. The hydroxyapatite was chosen as the carrier because of its adjustable acid–base properties, which are essential to the mechanism of this reaction. Several compositions of Pd(x)/CaHAp catalysts were synthesized and characterized by various spectroscopic techniques (XRD, IR, UV–visible), hydrogen temperature-programmed reduction (H_2-TPR), and hydrogen pulse chemisorption in order to correlate the MIBK production with the reducibility of the palladium dispersed on calcium hydroxyapatite. The acid–base properties of the catalyst were studied with the use of butan-2-ol conversion as the probe reaction.

2. Experimental

The calcium hydroxyapatite was synthesized by the double decomposition method, which is based on mixing a solution of ammonium hydrogenophosphate (0.4 M) with a solution of calcium nitrate (0.5 M) in the presence of ammonia. The solution containing the phosphate and ammonia is added dropwise to the boiling calcium nitrate solution. The resulting mixture was heated with reflux for 3 h and then filtered while it was hot. The recovered solid was thoroughly washed with ultrapure hot water to eliminate traces of nitrates and then dried at 373 K for 24 h and calcined at 673 K for 2 h in air.

Palladium-loaded hydroxyapatite was prepared by the conventional impregnation method with solutions of palladium nitrate containing different amounts of Pd. The resulting mixture was heated at 373 K until the water evaporated completely. The residue was calcined at 673 K for 2 h in a rotating reactor fed with air at 30 $cm^3\,min^{-1}$. The samples prepared contained 0.5–3 wt% palladium. They are designated Pd(x)/CaHAp, where (x) represents the percentage weight of Pd.

The specific surface area, along with pore size distribution and pore volume of the hydroxyapatite, was determined by nitrogen adsorption/desorption measurements at 77 K with a Sorptomatic 1900 Carlo Erba Instrument. Surface area was calculated with the BET equation [22]. Pore size distribution was deduced from the desorption curve of the isotherm, with the procedure developed by Barrett, Joyner, and Halenda (BJH) [23].

Chemical analyses of the samples were carried out by inductive coupling plasma–atomic emission spectroscopy (ICP-AES).

FTIR transmission spectra of CaHAp calcined at 673 K were recorded on a Bruker Equinox spectrometer in the 4000–400 cm^{-1} region, with the use of KBr discs. We investigated the acid–base properties of the catalysts by adsorbing 2.6-dimethylpyridine (also called lutidine; $pK_a = 6.7$) to self-supporting disks (10 mg) activated at 573 K in a vacuum (10^{-6} Torr) in a stainless-steel cell that allowed in situ analysis. Lutidine adsorption was carried out at room temperature and then desorbed at different temperature, and the IR spectra were recorded.

Diffuse reflectance spectra were recorded at room temperature between 190 and 2500 nm on a Varian Cary 5E

spectrometer equipped with a double monochromator and an integrating sphere coated with polytetrafluoroethylene (PTFE). PTFE was used as a reference.

Butan-2-ol conversion was studied in a continuous-flow reactor at atmospheric pressure in order to characterize the basic sites of the catalysts. The typical run was performed on 100 mg of the catalyst sieved to 120–180 µm. Butan-2-ol was supplied to the reactor diluted in nitrogen or air at a partial pressure of 8.4×10^2 Pa and at a total flow rate of 60 $cm^3\,min^{-1}$.

The Pd(x)/CaHAp catalysts were characterized by H_2-TPR (temperature-programmed reduction) measurements. The experiments were carried out with a Micromeritics Autochem 2910 apparatus equipped with a thermal conductivity detector. To minimize the contribution from adsorbed species, the samples (250 mg) were pretreated with O_2 (5% in He) at 673 K for 30 min, then were evacuated under an argon flow at 673 K and cooled to subambient temperature, 213 K. Such a low temperature is usually required to appreciate the reduction of noble-metal oxides dispersed on different substrates.

We started the TPR experiments by passing the gas mixture H_2 (5% in Ar, 50 $cm^3\,min^{-1}$) over the catalysts, while heating from 213 to 373 K at a rate of 5 $K\,min^{-1}$, then heating from 373 to 673 K at a rate of 10 $K\,min^{-1}$.

After the TPR, the catalysts were evacuated at 673 K under argon for 1 h, then cooled to 298 K and further evacuated at 298 K for 1 h. On the reduced samples, hydrogen pulse chemisorption experiments were performed to measure the accessible Pd sites and to determine the mean diameter of Pd particles (d_{Pd}). The analyses were carried out in a pulse flow system equipped with QMS and a thermal conductivity detector. Pulses of H_2 (5% in Ar, loop volume 0.5 cm^3) were injected at 343 K into the flow of argon (20 $cm^3\,min^{-1}$) until the breakthrough point was attained. Under these conditions, the partial pressure of hydrogen is almost 1 Torr, and at 343 K this low pressure prevents the formation of the β-hydride phase [24]. Successive injections of H_2 pulses produced peaks of different areas in the TCD signal. The catalyst metal surface was considered saturated when two consecutive peaks exhibited the same area. We shall denote the Pd dispersion by FE (fraction exposed), calculated by the formula $1.12/d_{Pd}$ (nm), assuming that palladium particles have a spherical shape [25].

The X-ray diffraction measurements for the structural determination were carried out with a Philips vertical goniometer and Ni-filtered Cu K_α radiation. A proportional counter and a 0.05° step size in 2θ, from $2\theta = 20°$ to 90°, were used. Crystalline phases were identified by comparison with ICSD reference files [26].

The catalytic tests of acetone condensation were performed in a U-shaped continuous-flow microreactor operated at atmospheric pressure with the use of 50–150 mg of the catalyst. Before each run the catalyst was reduced in situ at 673 K for 2 h by hydrogen at a flow rate of 30 $cm^3\,min^{-1}$. We supplied acetone diluted in 20 $cm^3\,min^{-1}$ of N_2 to the reactor at the reaction temperature (150 °C) by passing it through a saturator held at 273 K. The total flow rate was kept at 100 $cm^3\,min^{-1}$ by the addition of N_2 to the reaction mixture at the exit of the saturator. All of the experiments were carried out under the following conditions: $W/F = 20.50$ h g mol^{-1}, H_2/acetone = 1.05, and a reaction temperature equal to 423 K. Analysis of the reaction mixture was performed on a FID Unicam 610 chromatograph equipped with a 2-m (1/8 in.) stainless-steel column containing 10% Carbowax 20M on Chromosorb AW.

3. Results and discussion

3.1. Characterization of the samples

3.1.1. Morphological properties and chemical analyses of the CaHAp and Pd(x)/CaHAp catalysts

The morphological properties of the CaHAp and Pd(x)/CaHAp catalysts (such as specific surface area, mean pore size, and cumulative pore volume), along with the results of chemical analyses, are reported in Table 1. The CaHAp appears to be scarcely porous, as may be deduced from the adsoption/desorption isotherms (data not shown), with a very low contribution of the mesopores to the total surface area. The cumulative pore volume does not approach 0.1 $cm^3\,g^{-1}$ in the CaHAp. On this basis, the lack of dependence of surface area on the presence of Pd could be explained.

The chemical analyses show that the amount of Pd found in the samples is in agreement with the quantities introduced in solutions. The palladium loading does not significantly alter the specific surface area of the CaHAp. Moreover, it should be noted that the increase in Pd loading decreases the mean pore size, probably because the pores are partially packed with metal particles. This assumption is supported by the fact that generally the size of Pd particles is lower than or comparable to the dimensions of the average pore diameters of the carrier, with exception of highly palladium-loaded catalyst, Pd(3)/CaHAp, where Pd aggregates exceed the mean pore size of the support (see Tables 1 and 2). From these results it appears that the carrier pore sizes probably play a role in preventing metal particle agglomeration up to a certain Pd loading.

Table 1
Specific surface area and chemical analysis of the samples

Samples	Chemical analysis (wt% of Pd)		Surface area ($m^2\,g^{-1}$)	Mean pore size (nm)	Cumulative pore volume ($cm^3\,g^{-1}$)
	Theoretical	Observed			
Pd(0)/CaHAp	0	0	51.1	28.5	0.098
Pd(0.5)/CaHAp	0.5	0.48	48.8	28.2	0.094
Pd(1)/CaHAp	1	0.96	49.0	26.0	0.095
Pd(2)/CaHAp	2	1.96	48.0	25.0	0.088
Pd(3)/CaHAp	3	2.88	48.6	22.0	0.094

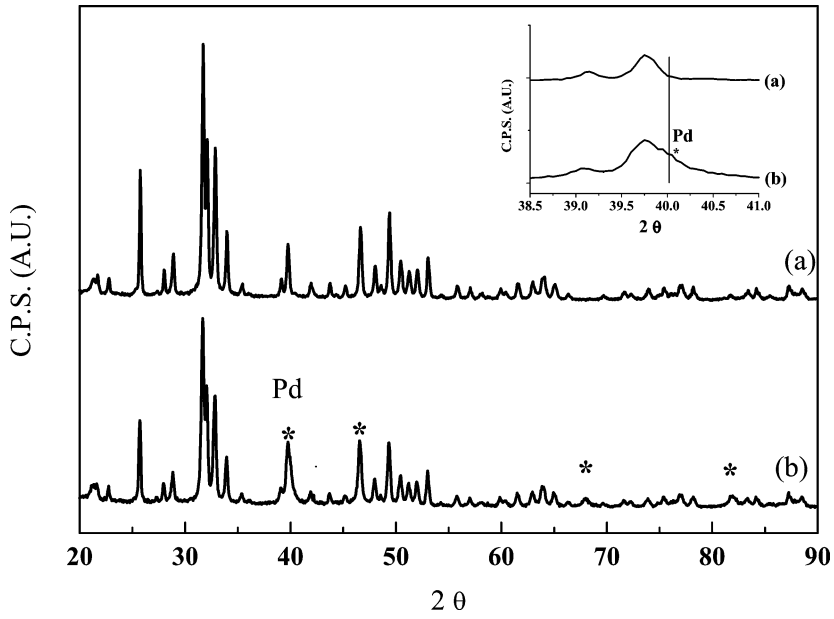

Fig. 1. XRD patterns of: (a) CaHAp and (b) Pd(2)/CaHAp after reduction at 673 K. (The inset is a magnification of the patterns (a) and (b) in the angular range 39°–41° (2θ), demonstrating the presence of Pd(111) peak.)

Table 2
Temperature-programmed reduction of Pd(x)/CaHAp

Catalysts	Temperature (K)		d_{Pd}[a] (nm)	Fraction of exposed Pd (F.E.)[b]	H_{ab}/Pd_t[c] atomic ratio
	I peak (H_2 uptake)	II peak (β-PdH decomposition)			
Pd(0.5)/CaHAp	276	337	8	0.32	0.14
Pd(1)/CaHAp	274	337	10	0.35	0.11
Pd(2)/CaHAp	269	338	20	0.39	0.06
Pd(3)/CaHAp	268	338	28	0.5	0.04
PdO[d]	280	360	–	–	–

[a] The mean Pd particle size (d) was determined by H_2 chemisorption pulses technique at 343 K and H_2 partial pressure of almost 1 Torr, in order to prevent the formation of β-PdH.

[b] The fraction of exposed (FE) Pd was calculated assuming spherical particle shape, by means of the expression $1.12/d_{Pd}$ (nm).

[c] In the atomic ratio H_{ab}/Pd_t, H_{ab} is the hydrogen absorbed (atoms per gram of catalyst) as β-PdH, below 300 K during the TPR, that desorbs at 337–338 K; Pd_t indicates the total amount of Pd (atoms per gram of catalyst).

[d] For comparison with the TPR of unsupported PdO, studied by Chou et al. [38].

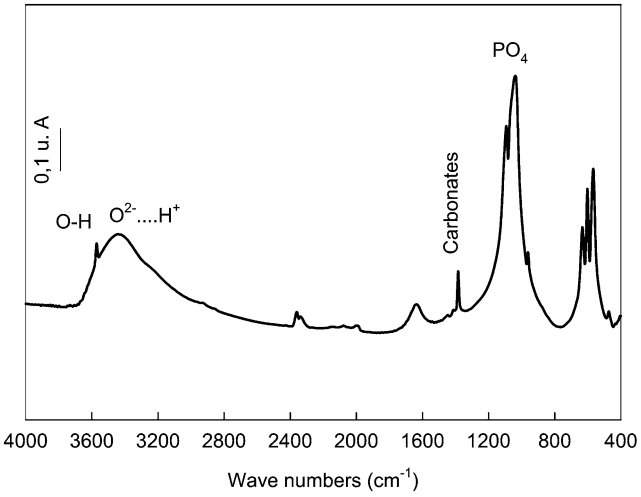

Fig. 2. IR spectra of CaHAp calcined at 673 K.

3.1.2. X-ray powder diffraction

The XRD patterns of the carrier CaHAp and of a selected reduced catalyst, Pd(3)/Hap, are shown in Fig. 1a and 1b, respectively. The diffractogram confirms that CaHAp calcined at 673 K is monophasic and has an apatitic structure. All of the peaks were indexed in the hexagonal system with the $P6_{3/m}$ space group (ICSD, no. 16742). The addition of Pd to CaHAp and the successive reduction treatments at 673 K do not visibly modify the structure of the support. A perusal of Fig. 1 (see the inset) indicates a broad peak around 40° (2θ), partially overlapped by the CaHAp signals, that can be ascribed to the peak (111) of metallic Pd (ICSD, no. 41517); additional features at about 68° and 82° (2θ) are also evident.

3.1.3. IR spectroscopy

The IR spectrum of CaHAp is composed of three domains (Fig. 2). The first one extends from 400 to 1200 cm^{-1} and contains the vibration modes of the P–O bond, which are characterized by three bands that appear at 965, 1035, and 1094 cm^{-1}. The absence of the band at 875 cm^{-1} usually attributed to $(HPO_4)^{2-}$ ions prevents the formation of pyrophosphates in the samples [20]. In the region of 1300–1600 cm^{-1} there are two bands located at 1395 and 1457 cm^{-1} that are attributed to carbonates and probably also to adsorbed CO_2, since the first band is shifted slightly toward low frequencies. The band appearing at 1642 cm^{-1}

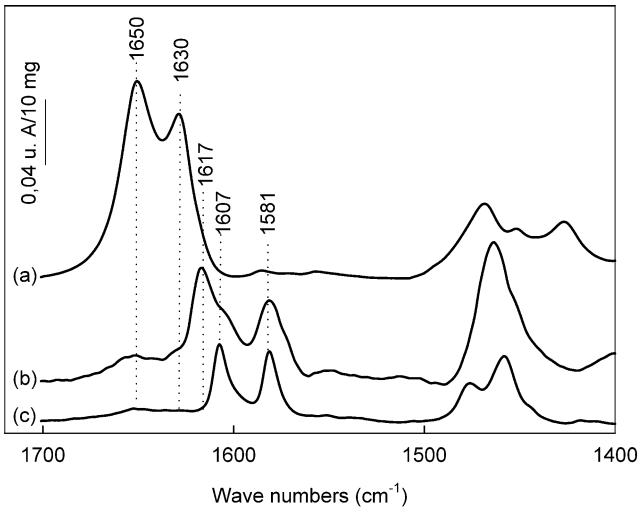

Fig. 3. IR spectra of lutidine adsorbed at room temperature then desorbed at 323 K over: (a) $AlPO_4$, (b) Al_2O_3, and (c) CaHAp.

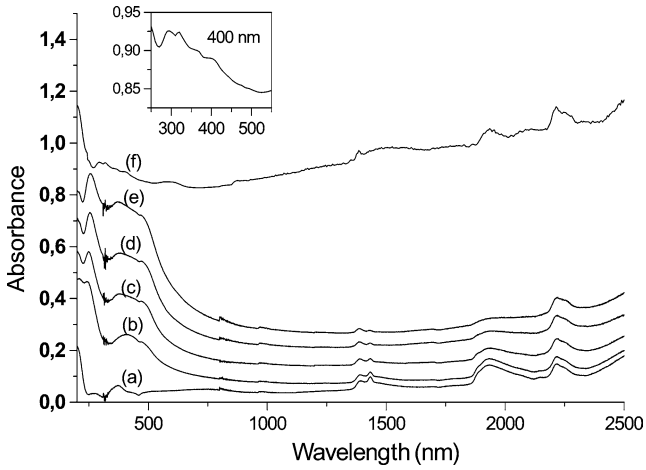

Fig. 4. UV–visible-NIR diffuse reflectance spectra of Pd(x)/CaHAp calcined under air at 673 K with different x (wt%) values: (a) $x = 0$; (b) $x = 0.5$; (c) $x = 1$; (d) $x = 2$; (e) $x = 3$; and (f) Pd(3)/CaHAp after reduction with H_2 at 673 K. (The inset shows the band of metallic Pd.)

is associated with that located at 3400 cm^{-1}, which is attributed to vibration modes of H_2O. The small and sharp band at 3566 cm^{-1} is due to the vibration modes of the O–H groups hosted by the apatite network.

To obtain further information on the nature and the strength of the acid sites of the calcium hydroxyapatite, we undertook an IR study of the interactions of the solid with lutidine. The collected results were compared with those obtained with Al_2O_3 and $AlPO_4$, which have specific surface areas and pore volumes of 220 $m^2\,g^{-1}$, 0.64 $cm^3\,g^{-1}$ and 215 $m^2\,g^{-1}$, 1.27 $cm^3\,g^{-1}$ respectively (Fig. 3). Usually lutidine adsorption gives rise to two bands at 1630 and 1650 cm^{-1}, characteristic of lutidinium ions interacting with Brønsted acid sites; a band at 1581 cm^{-1}; and another one located between 1607 and 1617 cm^{-1} typical of lutidine coordinated with Lewis acid sites. The surface of the band located at 1581 cm^{-1} is proportional to the number of Lewis acid sites, whereas the position of the second band is indicative of their strength [27]. The spectrum of Fig. 3a shows that $AlPO_4$ exclusively contains Brønsted acid sites, whereas alumina (Fig. 3b) bears primarily strong Lewis acid sites, which are associated with the band at 1617 cm^{-1}. The spectrum of calcium hydroxyapatite diluted in KBr displayed in Fig. 3c shows that it possesses a limited number of Brønsted acid sites. Concomitantly, the band appearing at 1581 cm^{-1} confirms that CaHAp also bears Lewis acid sites of moderate strength, identified by the band centered at 1607 cm^{-1}.

3.1.4. UV–visible NIR DRS

Complexes of Pd^{2+} (d^8) are generally square planar (and belong to the D_{4h} group of symmetry). The crystal field generated by the ligands consistently lifts the degeneracy, and the 4d level splits into several levels, whose increasing order of energy is $d_z^2 < d_{x.y} = d_{y.z} < d_{x.y} < d_{x^2-y^2}$. For complexes of the second and third series of transition metals, the strong field approach allows the following arrangement of levels: $a_{1g} < e_g < b_{2g} < b_{1g}$, which gives rise to the ground-state configuration: $(a_{1g})^2(e_g)^4(b_{2g})^2(b_{1g})^0$.

In D_{4h} symmetry, three spin-allowed transitions might be observed and three others are forbidden. The allowed transitions are $^1A_{1g} \rightarrow {}^1A_{2g}$; $^1A_{1g} \rightarrow {}^1E_g$; $^1A_{1g} \rightarrow {}^1B_{1g}$. The Pd complexes can also exhibit unusual symmetries, such as trigonal pyramidal (C_{3v}) or trigonal bipyramidal (D_{3h}), which are characterized by a ternary axis of symmetry. The splitting of d orbitals is qualitatively the same for all of the groups that have such a symmetry axis. The single electronic transitions then give rise to two spin-allowed transitions, $\nu_1 \equiv {}^1A_{1g} \rightarrow {}^1E_\alpha$ and $\nu_2 \equiv {}^1A_{1g} \rightarrow {}^1E_\beta$, and two spin-forbidden transitions, ν_1' and ν_2' [28,29].

The attribution of the observed bands with Pd(x)/CaHAp samples (Fig. 4) was performed by comparison with the spectra of reference compounds described in the literature. As an example, the spectrum of $Pd(NH_3)_4$ dispersed either on zeolites or on silica, recorded after an oxidation at 773 K, displays only two bands located around 280 and 480 nm [30,31]. With the alumina, depending on the nature of the used precursor, these bands appear around 260 and 440–460 nm. The first band is assigned to $O^{2-} \rightarrow Pd^{2+}$ charge transfers, and the second one, to $(\nu_1 + \nu_2)$ transitions arising from isolated species of palladium belonging to the C_{3v} symmetry group. On the other hand, according to Bozon-Verduraz [30], the diffuse reflectance spectrum of PdO prepared by direct oxidation of the metal presents three bands located at 260, 335, and 430 nm. Similar spectra were also obtained when PdO was synthesized by the oxidation of complexes such as $Pd(NH_3)(NO_2)_2$ or $Pd(Acac)_2$.

The spectrum of pure CaHAp is shown in Fig. 4a. It exhibits in the NIR at 1425 nm a band due to free OH groups of the hydroxyapatite and a two other bands located at 1385 and 1850–2100 nm attributed to adsorbed water. In the UV–visible region there is only a maximum around 200 nm due to $O^{2-} \rightarrow Ca^{2+}$ charge transfer. After CaHAp was loaded

with different amounts of palladium, the intensity of the bands of the hydroxyls in NIR decreased. Concomitantly, as the amount (x) of Pd was increased new bands appeared in the UV–visible region. For $x \leqslant 1\%$, the spectrum (Fig. 4b and 4c) contains only a broad band centered on 425 nm and two other bands at 250 and 200 nm. The bands centered at 250 and 200 nm are assigned to $O^{2-} \rightarrow Pd^{2+}$ and $O^{2-} \rightarrow Ca^{2+}$ charge transfers. The bands located at 425 nm correspond to the ν_1 ($^1A_{1g} \rightarrow {}^1E_\alpha$) and ν_2 ($^1A_{1g} \rightarrow {}^1E_\beta$) transitions due to dispersed PdO or isolated palladium species belonging to C_{3v} symmetry. This attribution is supported by the fact that CaHAp has ion exchange properties, and, therefore, it might not be excluded that a very small number of Pd^{2+} ions replace Ca^{2+} ions in the phosphate network.

Spectra of the samples containing palladium loadings greater than 1 wt% are displayed in Fig. 4d and 4e. They show bands at 275, 375, and 475 nm ascribable, as previously shown, to PdO. Therefore, the band at 275 nm is assigned to $O^{2-} \rightarrow Pd^{2+}$ charge transfers, the band at 375 nm is attributed to ν_3 ($^1A_{1g} \rightarrow {}^1B_{1g}$) transitions, and the broad band at 475 nm is associated with ν_1 ($^1A_{1g} \rightarrow {}^1A_{2g}$) and ν_2 ($^1A_{1g} \rightarrow {}^1E_g$) transitions.

The spectrum of the catalyst reduced by hydrogen at 763 K (Fig. 4) shows that the bands characteristic of palladium oxide disappeared totally and are replaced by a broad band centered around 350–400 nm, which is typical of metallic palladium [33].

3.1.5. H_2 temperature-programmed reduction and hydrogen pulse chemisorption

H_2 temperature-programmed reduction (TPR) experiments with Pd(x)/CaHAp were performed from 213 K up to 673 K. Fig. 5 displays a typical TPR profile for the catalyst Pd(3)/CaHAp. The temperatures of the peak maxima are given in Table 2.

During the TPR process, the reduction of palladium oxide species is expected to occur. Accordingly, the peak at 268 K, with a hydrogen uptake of 0.36 mmol g^{-1} of catalyst, may be attributed to the reduction of PdO crystallites not interacting with the support. The hydrogen uptake for this peak is higher than that expected for the reduction of all of the palladium, suggesting that concurrently with the metal reduction α- and β-hydride formation takes place [32–34]. A further increase in temperature determines in the TPR profile a negative peak, centered on 338 K, which is associated with β-PdH decomposition (0.068 $mmol_{H_2}\ g_{cat}^{-1}$). According to the phase diagram of the Pd–H_2 system [33], palladium crystallites, once reduced, tend to absorb hydrogen to form β-PdH, at low temperatures below 300 K and under a partial pressure of H_2 equal to 38 Torr (i.e., the P_{H_2} in our flow system H_2 (5% in Ar)). Then, as the temperature is raised to 337–338 K, palladium desorbs the absorbed hydrogen (denoted as H_{ab}), and a negative peak is observed in the TPR trace.

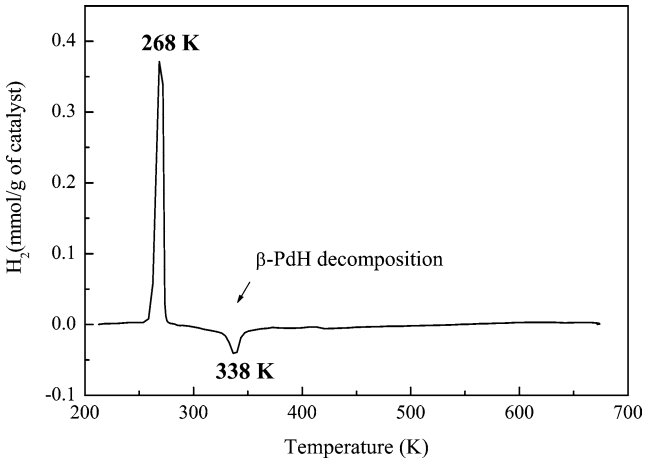

Fig. 5. TPR profile of oxidized catalyst Pd(3)/CaHAp.

It is known that the temperature and the shape of the peak of hydride decomposition are related to Pd dispersion on the carrier. It has also been established that Pd particle sizes are correlated with the stability of β-PdH and especially with the H/Pd ratio [32–34]. To obtain additional information on the mean diameter of Pd particles, the H_{ab}/Pd_t ratios were calculated from the hydride decomposition peaks (as atoms of absorbed hydrogen/atoms of Pd per gram of catalyst; see Table 2). It can be noticed that the H_{ab}/Pd_t ratio increases when the exposed fraction of Pd decreases. In the case of the Pd(3)/CaHAp sample, this ratio approaches a value close to that usually used for bulk β-PdH [35]. On the other hand, the position of the minimum of the hydride decomposition peak does not seem to depend on the extent of Pd dispersion (see Table 2).

Recently, the reduction of supported and unsupported PdO has been widely investigated [36–38], and our results are in line with those reported in the literature (see Table 2).

Hydrogen chemisorption pulses (at 343 K and a partial pressure of hydrogen of almost 1 Torr) over the reduced catalysts allowed measurement of the accessible Pd surface. Taking into account that the stoichiometry factor between the adsorbed hydrogen and the active metal is 2, the Pd particle sizes have been calculated along with the metal fraction exposed (FE) (see Table 2). In the series Pd(x)/CaHAp, the diameter (d_{Pd}) of palladium varies from 8 to 28 nm and, as expected, increases with the metal loading.

3.1.6. Butan-2-ol conversion

Calcium hydroxyapatite is known to exhibit basic properties that might play a role in the processes involved in the acetone transformation into MIBK. To investigate these acid–base features at the "working" temperatures of the catalysts, butan-2-ol conversion was used as the probe reaction [39]. The dehydration reaction leads to an ether or/and an olefin on acid sites and to a ketone by dehydrogenation on basic or redox sites in the presence of oxygen. Fig. 6 displays the variations of butan-2-ol conversion to methyl ethyl ketone versus the reaction temperature over pure CaHAp in the absence and the presence, respectively, of oxygen in the reaction mixture. In the absence of O_2 (Fig. 6a), the activ-

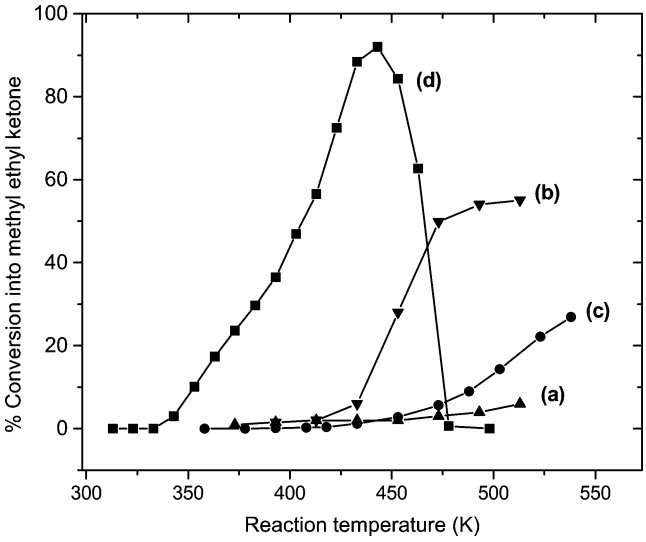

Fig. 6. Butan-2-ol conversion into methyl ethyl ketone over CaHAp: (a) in the absence and (b) the presence of O_2 and over Pd(1)/CaHAp: (c) in the absence and (d) the presence of O_2.

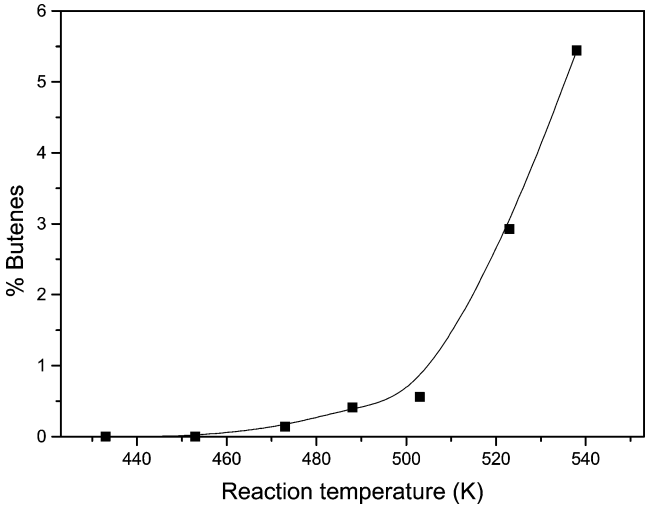

Fig. 7. Butan-2-ol conversion into butenes in the absence of O_2 on Pd(1)/CaHAp.

ity is low and exclusively oriented toward the production of methyl ethyl ketone (about 3% at 513 K). Addition of oxygen improves remarkably the dehydrogenation reaction, leading to about 50% butan-2-ol conversion to methyl ethyl ketone at 503 K (Fig. 6b). The butene production never exceeds 6%, even at 533 K. No formation of CO_2 was detected at the investigated temperatures. These results suggest that the calcium hydroxyapatite has a prevailing basic character, since it is principally active in dehydrogenation. The presence of a limited number of acid sites can be taken into account for the butene production. Moreover, on the basis of the results reported so far, it may be inferred that the basic sites of calcium hydroxyapatite are not directly involved in the reaction mechanism, since without O_2 their activity is very limited. They are probably constituted by oxygen species bonded to Ca^{2+} ions located near the tunnels of the structure. Such a type of oxygen, previously identified by ESR studies [40], is known to play a role in the catalytic processes.

With the Pd-loaded CaHAp catalysts the global conversion of the alcohol is notably increased (Fig. 6c and 6d). In the absence of oxygen the dehydration reaction starts around 443 K and increases regularly with the temperature reaching over Pd(1)/CaHAp a conversion into butenes of 55% at 533 K (Fig. 7). Introduction of O_2 to the reaction mixture does not noticeably modify the butene production and, therefore, the acid properties of the surface. Concurrently, the dehydrogenation activity over redox sites increases markedly. It starts, as shown on Fig. 6d, at much lower temperatures (around 343 K) than on the pure hydroxyapatite. The production of methyl ethyl ketone increases rapidly with the temperature and reaches almost 100% at 443 K. Above this temperature the yield of methyl ethyl ketone decreases because the reaction products are completely oxidized into CO_2. In the presence of oxygen and above 443 K, the redox properties of palladium prevail over all of the other characteristics of the catalyst.

3.2. Acetone condensation

The one-step selective conversion of acetone into MIBK requires, as reported in the literature, bifunctional catalysts containing a hydrogenating metal dispersed on a large-surface-area carrier [6–11]. The carrier and the metal often interact and develop cooperative effects that most times improve the performance of the system. These synergetic aspects of bifunctional catalysis have been widely discussed in several reviews [41,42]. In the case of the reaction studied here, the metal activates hydrogen, which diffuses toward the neighboring basic sites of the phosphate surface on which two adsorbed acetone species will be hydrogenated to yield MIBK [43]. Pure calcium hydroxyapatite submitted to a reaction mixture free of H_2 has a very low conversion, even at 423 K (1.5%), and produces only DAA and MO with selectivity approaching 9.8 and 90.2%, respectively. Therefore, since it is commonly admitted that MO is the main by-product that leads by hydrogenation to MIBK, the Pd(x)/CaHAp catalyst possesses all of the features required for an efficient reaction.

3.2.1. Product distribution

The condensation of acetone and its conversion into MIBK have been widely investigated in liquid phase with the use of different basic catalysts [4,5]. The products of the reaction are mainly diacetone alcohol and mesityl oxide, with a global conversion approaching 20%. Over Pd(x)/CaHAp and in gas phase the reaction produces mainly propan-2-ol (2P), methyl isobutyl ketone (MIBK), methyl isobutyl carbinol (MIBC), diisobutyl ketone (DIBK), traces of diacetone alcohol (DAA), and mesityl oxide MO (with conversions ranging between 0.2% and 22%). Fig. 8 reports the product distribution versus the conversion and shows that

the major products are MIBK and MIBC, even at the highest conversions reached.

The DAA and MO are intermediate products, since their yields exhibit a maximum versus conversion. They result, respectively, from the hydrogenation of one or two condensed molecules of acetone over Pd particles. Below a conversion of 10% these products are not detected. As the conversion increases the MIBK tends to become a secondary product because, as shown by the reaction pathway (Fig. 9), it is transformed by subsequent hydrogenation into MIBC or by condensation into DIBK. All of these considerations can be confirmed by the computation, for each compound, of the tangent at the origin, which obviously is equal to zero for by-products.

3.2.2. Influence of residence time

Fig. 10 depicts the dependence of acetone conversion and product selectivity on the contact time (W/F_{ac}) for the Pd(2)/CaHAp catalyst. It shows that the conversion increases in a hyperbolic way as W/F is increased. It does not seem to reach a maximum in the domain of the investigated residence time, suggesting that the reaction is not of zero order. Moreover, with the aim of circumventing the limitation of the reaction kinetics by secondary phenomena such as matter transfers or diffusion, the experiments were carried out after determination of the adequate catalyst grain size, the length of the catalytic bed, and the valid flow rates of the reaction mixture, for a residence time below 20 g h mol^{-1}.

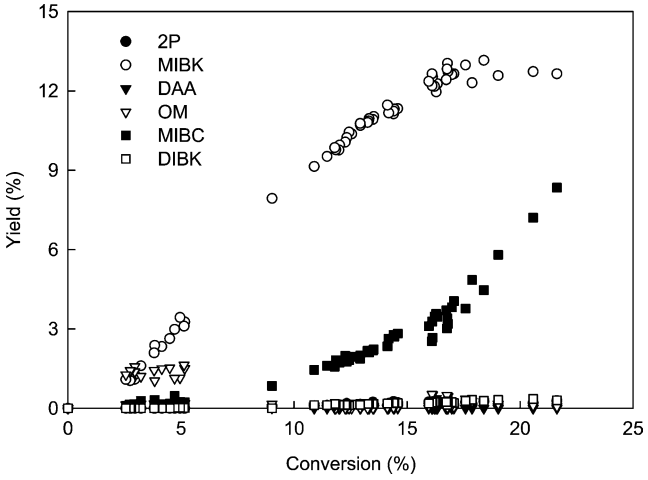

Fig. 8. Distribution of the products of acetone condensation versus the conversion over Pd(2)/CaHAp.

3.2.3. Stability of the catalysts

Fig. 11 shows the variations in acetone conversion versus time over Pd(2)/CaHAp. The loaded palladium exhibits, under the chosen reaction conditions, good stability, since no significant decay of activity was observed. The water produced by the reaction does affect the catalyst behavior and does not seem to destroy the basic properties of the CaHAp. After more than 3 h on stream the conversion stabilizes around 17%. No sintering or excessive formation of carbonaceous deposits was directly observed on the catalyst surface.

The selectivity of the products increases slightly at the beginning of the reaction; however, MIBK (66.4%) and MIBC (28.3%) remain the main products. The global selectivity for the by-products, propan-2-ol and DIBK, does not exceed 5.3%.

3.2.4. Influence of reaction temperature

Fig. 12 displays the global conversion and the product selectivity versus reaction temperatures. Except for MIBK, all of the conversions exhibit a maximum. To verify that this maximum is not due to secondary phenomena such as the presence of an impurity in the feeding mixture, we determined the conversions at first by increasing the reaction temperature and then decreasing it. As a matter of fact, it was

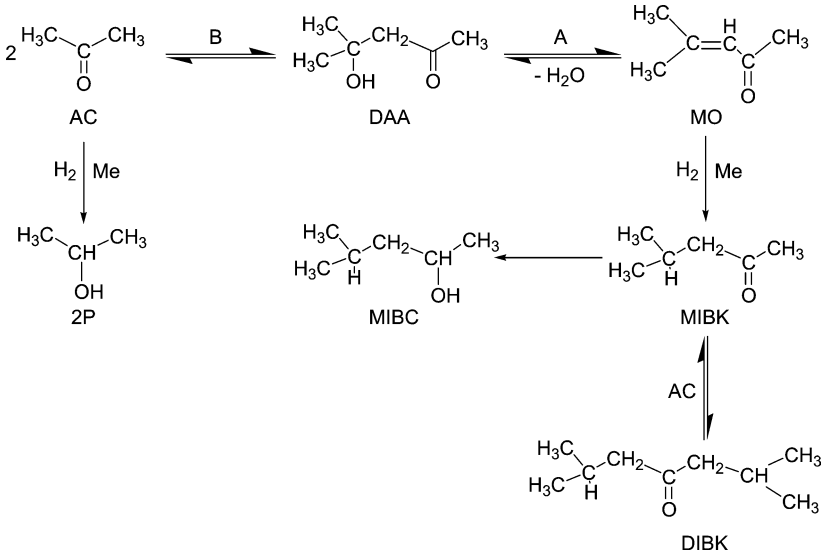

Fig. 9. Simplified scheme of the reaction of acetone with hydrogen on a solid catalyst (A: acid sites; B: basic sites; Me: hydrogenating metallic sites).

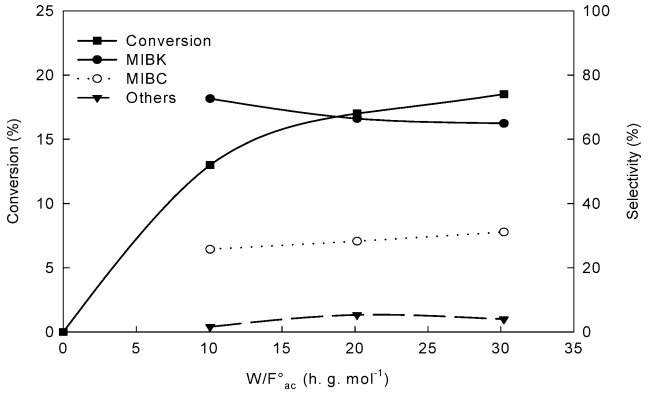

Fig. 10. Influence of residence time over acetone conversion on Pd(2)/CaHAp.

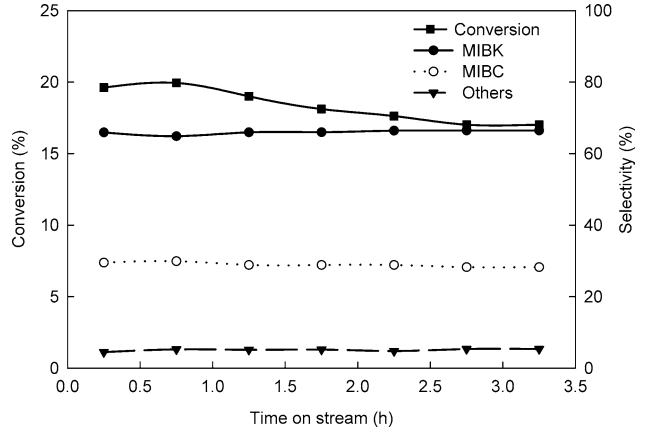

Fig. 11. Variation of the conversion and the selectivity of the reaction products versus time on stream over Pd(2)/CaHAp.

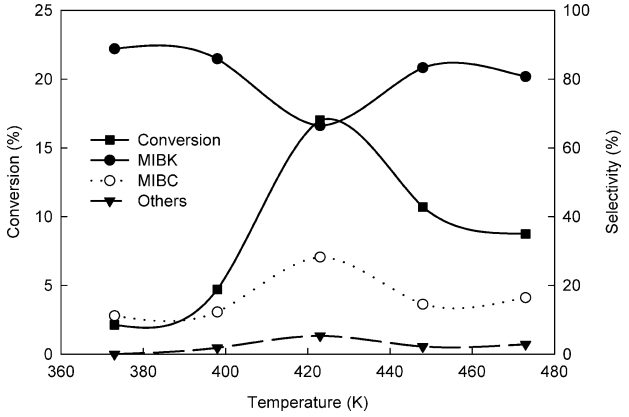

Fig. 12. Global conversion of acetone and selectivity of the products versus the reaction temperature over Pd(2)/CaHAp.

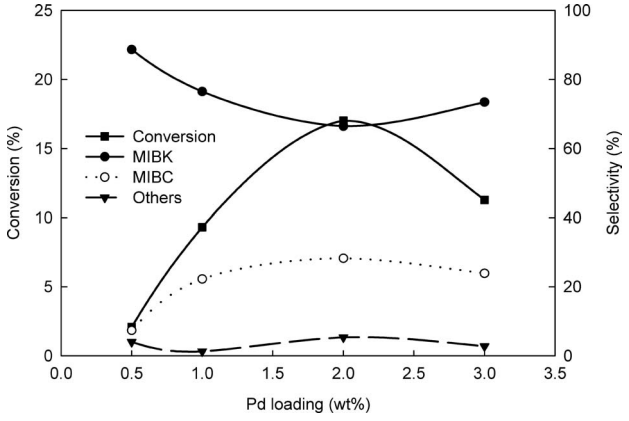

Fig. 13. Conversion and selectivity over Pd(x)/CaHAp versus palladium loading.

found for a number of hydrogenation reactions (such as ethylene hydrogenation) that the appearance of a maximum in the catalyst activity is not due to thermodynamic limitations but to new active sites created by traces of oxygen in the reaction mixture [44]. The results displayed in Fig. 12 show that the global conversion increases with the temperature and describes the same maximum (located at 423 K) as when the conversion is measured during a decrease in the temperature. The decrease in activity, observed after the maximum, is attributed to a decrease in the density of basic sites that are involved in the condensation of acetone. This step is supposed to be the limiting one in the reaction mechanism and the kinetics of MIBK production.

The selectivities of the products, except that of MIBK, present analogous profiles. The MIBK exhibits a minimum when the global conversion is at the maximum. This result suggests that the hydrogenation of MIBK into MIBC is supported by the high conversion of acetone.

3.2.5. *Effect of palladium content*

Fig. 13 shows the variations in the conversion and the product selectivities versus the amount of loaded palladium over CaHAp. The conversion and the selectivity are both maximum for 2 wt% Pd. The selectivities for the reaction products, except for MIBK, are also maximum for this Pd loading. The formation of secondary products by a further hydrogenation of MIBK is favored by the increase in Pd content. However, the production of these compounds does not significantly modify the global conversion. Similar behavior was reported by Watanabe et al. [45] in their study of the influence of palladium loading on the activity of Pd/ZrP [44]. This increase in the amount of Pd increases the selectivity for propan-2-ol at the expense of that for MIBK and DIBK. Yang and Wu reported analogous results over Pd/SAPO catalyst, which possesses pronounced acid properties [46]. On the other hand, Das and Srivastava have found equivalent results over Pd/MgAl(O), which has basic features [37]. They attributed the decrease in the selectivity to the agglomeration of Pd particles over the basic sites, which are believed to be the active sites in the acetone condensation. There is probably an adequate ratio between the basic sites and the hydrogenating metallic sites, leading to optimal performances. In the case of the results reported here, it seems that the selectivity principally depends on the size of the Pd particles. It was previously shown (Table 2) that the palladium agglomeration increases with

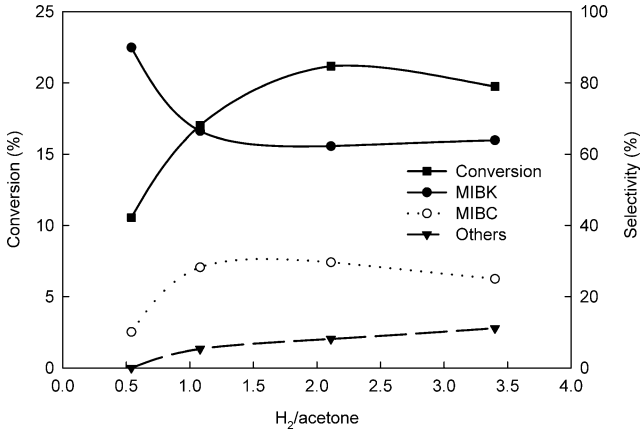

Fig. 14. Conversion and selectivity versus H_2/acetone over Pd(2)/CaHAp.

the increase in loading. The aggregation of these particles affects the catalyst performance by decreasing the MIBK selectivity from 90 to 75%, when, for instance, the crystallite size increases from 8 nm in Pd(0.5)/CaHAp to 28 nm in Pd(3)/CaHAp.

3.2.6. Effect of H_2/acetone ratio on selectivity

Fig. 14 displays the changes in the conversion and the selectivity over Pd(2)/CaHAp versus the composition of the feeding mixture expressed as the H_2/acetone ratio. It shows that the global conversion increases while the ratio increases and reaches an optimum value for a H_2/acetone ratio equal to 2. Concomitantly, the MIBK conversion decreases and stabilizes in agreement with the stoichiometry of the reaction of MIBK production. The same optimum value was obtained by Yang and Wu in their study of the reaction over Pd/SAPO [46].

4. Conclusion

From all of the results presented above, the following conclusions were drawn:

- Butan-2-ol conversion and IR spectroscopy, coupled with the lutidine adsorption/desorption, showed that calcium hydroxyapatite bears acid and base sites. Its specific surface area was found not to be notably affected by the impregnation process with palladium. The loaded PdO is easily reducible at low temperatures and is well dispersed on the carrier.
- The reaction parameters, such as the temperature, the residence time, the H_2/acetone ratio, and the amount of loaded Pd, play an important role in MIBK production. The production of MIBK exhibits an optimum versus the temperature.
- Pd/CaHAp is selective in the production of MIBK and MIBC. At a conversion of 22% the selectivity for these two products is equal to 92%. Propan-2-ol and DIBK are also produced, but in negligible amounts. The absence of diacetone alcohol in the reaction products, even at high conversion, suggests that it is dehydrogenated over the acid sites of the CaHAp. The catalyst does not produce mesityl oxide, because it is immediately hydrogenated into MIBC.

References

[1] Ullman's Encyclopaedia of Industrial Chemistry, vol. A 105, 1990, p. 79.
[2] K. Weisermel, H.J. Apre, Industrial Organic Chemistry, Important Raw Materials and Intermediates, A. Muller (translator), VCH, New York, 1978, p. 247.
[3] Y. Higashio, T. Nakayama, Catal. Today 28 (1996) 127.
[4] K. Othmer, Encyclopaedia of Chemical Technology, vol. 13, Wiley, New York, 1979, p. 907.
[5] T. Maki, T. Yokoyama, Y. Sumino, Ipn. Pat. 6396147 (1988) to Mitsubishi Chemical Industries Co., Ltd.
[6] R. Unnikrishnan, S. Narayanan, J. Mol. Catal. A Chem. 144 (1999) 173.
[7] L. Melo, G. Giannetto, F. Alvarez, P. Magroux, M. Guisnet, Catal. Lett. 44 (1997) 201.
[8] K.H. Lin, A.N. Ko, Appl. Catal. A 147 (1996) L259.
[9] Y.Z. Chen, B.J. Liaw, H.R. Tan, K.L. Shen, Appl. Catal. A 205 (2001) 61.
[10] A.A. Nikopolus, G.B. How, W.L. Jang, R. Subramanian, J.J. Spivey, D.J. Olsen, T.J. Devon, R.D. Culp, in: M.E. Ford (Ed.), Catalysis of Organic Reactions, Dekker, New York, 2000, p. 533.
[11] N. Das, D. Tishit, R. Durand, P. Greffen, B. Coq, Catal. Lett. 71 (2001) 181.
[12] J.C. Védrine, Phosphorus Res. Bull. 10 (1999) 37.
[13] M. Wakamura, K. Kandori, T. Ishikawa, Colloids Surf. 164 (2000) 297.
[14] J.A.S. Bett, W.K. Hall, J. Catal. 10 (1968) 105.
[15] C.L. Kibby, W.K. Hall, J. Catal. 29 (1973) 144.
[16] N.S. Figoli, H.R. Keslman, P.C. L'Argentier, C.L. Lazzraoui, J. Catal. 77 (1982) 64.
[17] A. Elazarifi, A. Elouassili, M. Lakhdar, A. Essamarty, J. Van Gestel, J. Leglise, Phosphorus Res. Bull. 10 (1999) 930.
[18] St. Naray-Szabo, Zeitsch-Krist. 75 (1930) 323.
[19] C.A. Beevers, D.B. McIntyre, Miner. Mag. 27 (1945) 254.
[20] J.C. Elliot, Structure and Chemistry of the Apatites and Other Calcium Orthophosphates, Elsevier, Amsterdam, 1994.
[21] S. Sugiyama, H. Matsumoto, H. Hayashi, J.B. Moffat, Colloids Surf. 169 (2000) 17.
[22] S. Brunauer, P.H. Emmet, E. Teller, J. Am. Chem. Soc. 60 (1938) 309.
[23] E.P. Barrett, L.G. Joyner, P.P. Halenda, J. Am. Chem. Soc. 73 (1953) 373.
[24] P.C. Aben, J. Catal. 10 (1968) 224.
[25] S. Ichikawa, H. Poppa, M. Boudart, J. Catal. 91 (1985) 1.
[26] Inorganic Crystal Structure Data Base (ICSD), National Institute of Standards and Technology (NIST), release 2004/2.
[27] H. Miyata, J.B. Moffat, J. Catal. 62 (1980) 357.
[28] M. Lvubosky, L. Pfefferle, Catal. Today 47 (1999) 29.
[29] A. Rakai, A. Bensalem, J.C. Muller, D. Tessier, F. Bozon-Verduraz, in: L. Guczi, F. Solymosi, P. Tetenyi (Eds.), Proceedings of the 10th International Congress on Catalysis, 19–24 July 1992, Budapest, Hungary, in: New Frontiers in Catalysis, Elsevier, Amsterdam, 1993.
[30] A. Rakai, D. Tessier, F. Verduraz, New J. Chem. 16 (1992) 869.
[31] Y. Yazwa, H. Yoshida, N. Takagi, S. Komai, A. Sutsuma, T. Hottori, J. Catal. 187 (1999) 15.
[32] M. Boudart, H.S. Hwang, J. Catal. 39 (1975) 44.
[33] F.A. Lewis, The Palladium/Hydrogen System, Academic Press, New York, 1967.

[34] A.L. Bonivardi, M.A. Baltanás, J. Catal. 138 (1992) 500.
[35] J.J.S. Scolten, J.A. Konvalinka, J. Catal. 5 (1966) 1.
[36] A. Benedetti, G. Fagherazzi, F. Pinna, G. Rampazzo, M. Selva, G. Strukul, Catal. Lett. 10 (1991) 215.
[37] N.N. Das, S.C. Srivastava, Bull. Mater. Sci. 25 (4) (2002) 283.
[38] C.W. Chou, S.J. Chu, H.J. Chiang, C.Y. Huang, C.J. Lee, S.R. Sheen, T.P. Perng, C.T. Yeh, J. Phys. Chem. B 105 (2001) 9113.
[39] Y. Brik, M. Kacimi, F. Bozon-Verduraz, M. Ziyad, Micropor. Mesopor. Mater. 43 (1) (2003) 101.
[40] Y. Matsumura, H. Kanai, J.B. Moffat, J. Mol. Catal. A 115 (1997) L229.
[41] M. Boudart, Adv. Catal. 20 (1969) 153.
[42] P.B. Weisz, Adv. Catal. 13 (1962) 137.
[43] R. Unikrishnan, S. Narayanan, J. Mol. Catal. 144 (1998) 173.
[44] J.W. May, Adv. Catal. 21 (1970) 151.
[45] Y. Watanabe, Y.M. Matsumura, Y. Izumi, Y. Mizutani, J. Catal. 40 (1975) 76.
[46] S.M. Yang, Y.M. Wu, Appl. Catal. 192 (2000) 211.